Hindawi Publishing Corporation
Journal of Sensors
Volume 2009, Article ID 637874, 10 pages
doi:10.1155/2009/637874

Review Article

Integrated MEMS/NEMS Resonant Cantilevers for Ultrasensitive Biological Detection

Xinxin Li,[1] Haitao Yu,[1] Xiaohua Gan,[1] Xiaoyuan Xia,[1] Pengcheng Xu,[1] Jungang Li,[1] Min Liu,[1] and Yongxiang Li[2]

[1] *State Key Lab of Transducer Technology, Shanghai Institute of Microsystem and Information Technology, Chinese Academy of Sciences, 865 Changning Road, Shanghai 200050, China*
[2] *State Key Lab of High Performance Ceramics and Superfine Microstructures, Shanghai Institute of Ceramics, Chinese Academy of Sciences, 1295 Dingxi Road, Shanghai 200050, China*

Correspondence should be addressed to Xinxin Li, xxli@mail.sim.ac.cn

Received 6 January 2009; Accepted 14 April 2009

Recommended by Michele Penza

The paper reviews the recent researches implemented in Chinese Academy of Sciences, with achievements on integrated resonant microcantilever sensors. In the resonant cantilevers, the self-sensing elements and resonance exciting elements are both top-down integrated with silicon micromachining techniques. Quite a lot of effort is focused on optimization of the resonance mode and sensing structure for improvement of sensitivity. On the other hand, to enable the micro-cantilevers specifically sensitive to bio/chemical molecules, sensing materials are developed and modified on the cantilever surface with a self-assembled monolayer (SAM) based bottom-up construction and surface functionalization. To improve the selectivity of the sensors and depress environmental noise, multiple and localized surface modifications are developed. The achieved volume production capability and satisfactory detecting resolution to trace-level biological antigen of alpha-fetoprotein (AFP) give the micro-cantilever sensors a great promise for rapid and high-resoluble detection.

1. Introduction

For recognition and detection of individual cells and bio/chemical molecules, micromechanical cantilever sensors with picogram to femtogram mass-sensing resolution in air environment have been attracting intensive researches [1]. According to measurement scheme, sensing mechanism of the micromechanical cantilevers can be categorized into static and dynamic detecting methods. With the static detecting method, the target molecules are detected by measuring cantilever surface stress, which is induced by specific bio/chemical binding or interaction at the surface of the cantilever [2–6]. Differently, the dynamic detecting method employs the cantilever as a resonator. Induced by specific mass adsorbate, a shift in the resonant frequency is read out as the sensing signal [7–11].

The pioneer investigation by Thundat et al. demonstrated the mass-sensing capability of micromechanical resonant cantilevers [7]. With precise optical detection of atomic force microscopy (AFM), a single cell or virus has been sensed in air environment [8, 9]. In ultrahigh vacuum, the resonant cantilevers even showed the mass resolution as high as attogram level [10]. However, these previously reported results were generally obtained in laboratories, with an off-sensor optical position sensing detection (PSD) of AFM mode used [11, 12]. For portable bio/chemical sensing applications, there is a recent trend to integrate the sensing and actuating elements into the cantilever for on-chip dynamic detection [6, 13, 14].

For static detection, the whole surface of one side of the cantilever is coated with a sensing layer, that is, affinity to the targeted analyte, while the other side is relatively passive. The specific reaction or combination between the analyte and the sensing layer can cause surface stress on the cantilever that gives rise to a bending of the cantilever [1, 4, 15, 16]. For a resonant cantilever, however, the sensing area would be better to be localized near the free end to enhance the mass loading signal and to depress cross-talk signal from spring-constant change.

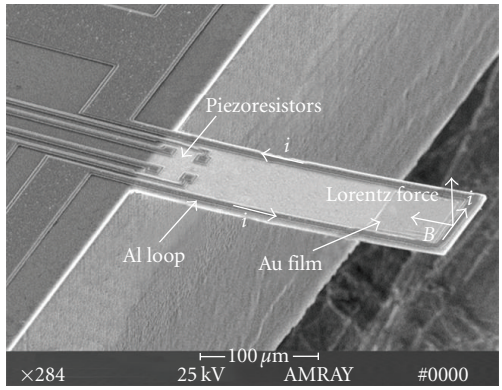

Figure 1: SEM image of the integrated resonant piezoresistive cantilever with the electromagnetic excitation schemes denoted.

For on-the-spot portable detection, microcantilevers integrated with on-chip read out are highly in demand. For example, piezoresistive read out based on measuring the bending stress of the cantilever is a suitable approach [17–19]. Using the piezoresistive cantilevers, chemical vapors have been detected with high sensitivity [20–22]. It is worth to point out that these previously developed piezoresistive microcantilevers, more often than not, comprised polysilicon piezoresistors in silicon nitride cantilever or doped single-crystalline silicon piezoresistors in silicon cantilever. For the former, the piezoresistive sensitivity of the polysilicon is lower compared to its single-crystalline counterpart [23]. For the latter, p-n junction isolation is generally used for the single-crystalline piezoresistors. Electronic noise relative to p-n junction current leakage is inevitable that more or less lowers the detecting resolution. For a static surface-stress sensing cantilever, the noise will directly degrade the detection resolution. For a resonant cantilever sensor, however, frequency shift is used to characterize the sensing signal and the noise in the piezoresistive output only indirectly influence the sensor performance. As long as the resonant amplitude of the cantilever is high enough, the piezoresistive output voltage can safely surpass the noise level and the frequency shift can be precisely read out.

Both resonant and static cantilever sensors have been developed in the State Key Lab of Transducer Technology located at Shanghai branch of Chinese Academy of Sciences. This review paper will mainly address the technical details and achievements about the resonant cantilevers and their biological sensing applications recently obtained in our lab.

2. Formation of the Integrated Resonant Cantilevers

Developed in the State Key Lab of Transducer Technology, the SEM image of an integrated silicon cantilever sensor is shown in Figure 1 for description of our design [24]. The piezoresistive sensing scheme and the electromagnetic excitation are utilized for the resonant cantilevers sensors. A small-bulk NdFeB magnet, purchased from Beijing Zhong Ke San Huan High-Tech Co., is mounted in the sensor package to generate magnetic field of about 50 mT for Lorentz-force excitation. The magnet generated magnetic field is measured with a 3G-3-A Tesla-meter. When a *sine*-wave AC electric current is fed through the aluminum loop, the cantilever will vibrate under the Lorentz force. The driving force is located at the cantilever end, that is, the peak location of the 1st resonant mode. The piezoresistive wheatstone bridge for frequency signal read out is put near the cantilever root, where maximum vibration-induced stress is located.

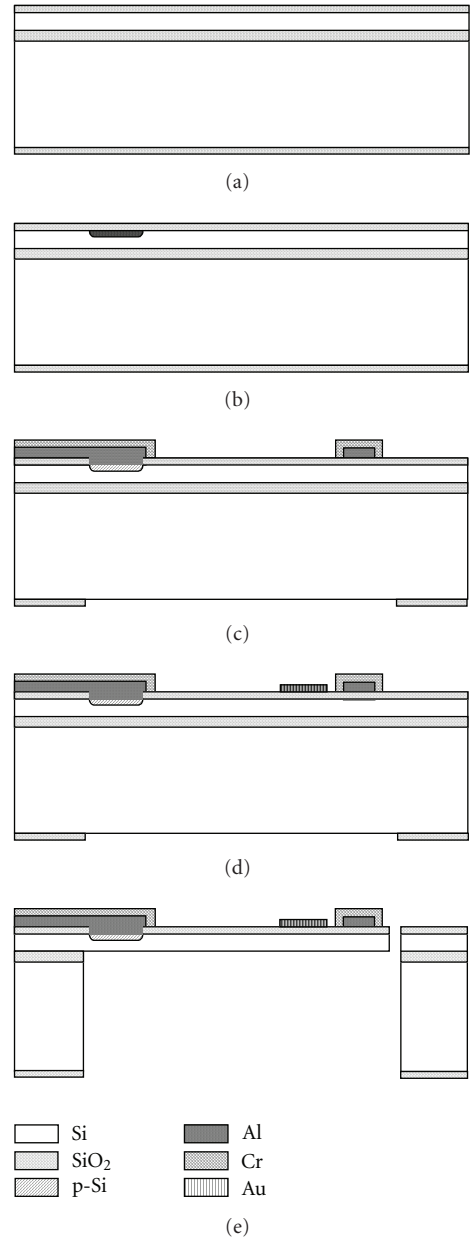

Figure 2: Fabrication processes of the integrated cantilever.

Considering the surface area for mass adsorption and the configuration of the piezoresistors and the Lorentz-coil, identical dimension of $300 \times 100 \times 3\,\mu m^3$ is designed. The calculated effective mass is 52.5 pg. The eigen-frequency for

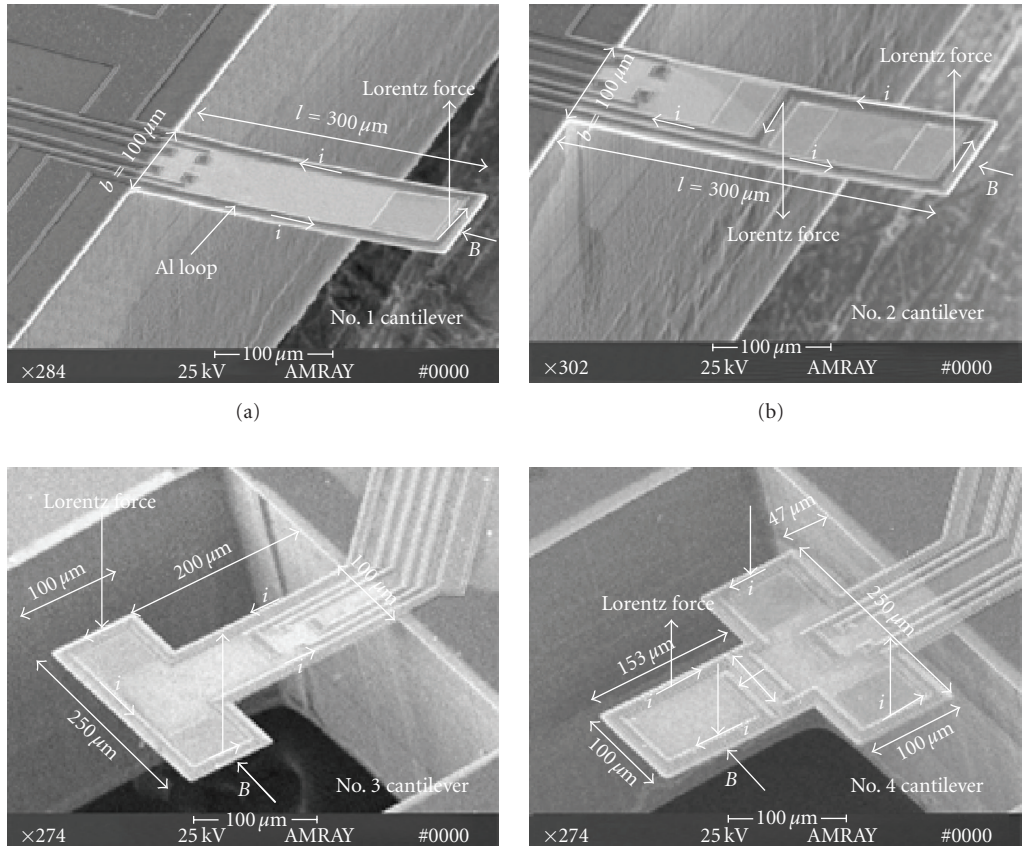

Figure 3: SEM images of the fabricated microcantilevers with the dimensions denoted. For the cantilevers from "a" to "d," their resonance modes are the 1st flexure-mode, the 2nd flexure-mode, the 1st torsion-mode, and the 2nd torsion-mode, respectively.

the fundamental resonance mode is designed as 45.9 KHz. The sensitivity is calculated as 0.43 Hz/pg.

With the main process steps shown in Figure 2, the cantilever fabrication starts from (100) silicon on insulator (SOI) wafers, with 3.1 μm-thick 1–10 $\Omega \cdot$ cm n-type top-layer and 0.36 μm-thick buried oxide (BOX) layer [25]. (1) A 2000 Å-thick SiO_2 layer is grown by dry oxidation. (2) By ion implantation, boron doping for the piezoresistor is implemented with 150 Ω targeted sheet-resistance. (3) Contact holes are opened and Al interconnection is processed. For protecting the Al from being damaged during the following cantilever gold-surface cleaning with H_2SO_4 + H_2O_2, an extra Cr layer is sputtered and patterned to cover the Al lines. (4) To immobilize a sensing film for specific molecular adsorption, 10 nm-thick Cr adhesion layer and 30 nm Au film are sequentially coated by using electron-beam evaporation. Then the Cr/Au sensing pads are formed at the cantilever-paddle terminals by lift-off process. (5) The ⟨100⟩-oriented cantilever is shaped by front-side reactive ion etching (RIE) and backside deep RIE, respectively. The cantilever is released by removing the BOX-layer with HF. The SEM image of the fabricated cantilever is shown in Figure 1.

3. Resonance Mode Optimization of Dynamic Microcantilevers

Micromechanical resonant cantilever sensors are operated by detecting frequency shift, that is, directly induced by an additional mass. The detecting resolution of the resonant frequency, which determines the sensing resolution for mass adsorption, can be improved by enhancing the Q-factor value [26]. Most of practical resonant cantilever sensors need to be operated in atmosphere air where a large volume air is surrounding the cantilever. Therefore, air-drag energy loss is the main factor to limit the Q-factor of microscale resonant cantilever in air, and thus dominates the mass-sensing resolution. Resonance-mode optimization is found to be effective in improving the Q-value and mass sensing resolution. There have been individual reports on individual experimental findings of resonance-mode influenced sensing performance [27, 28]. Recently, we carried out a systematic study to reveal the effect of different orders of resonance modes of microcantilevers on Q-value and mass-sensing resolution [29].

We use theoretical analysis, finite-element simulation, and experimental measurement to investigate the air drag damping effect on Q-factor of the cantilevers in various

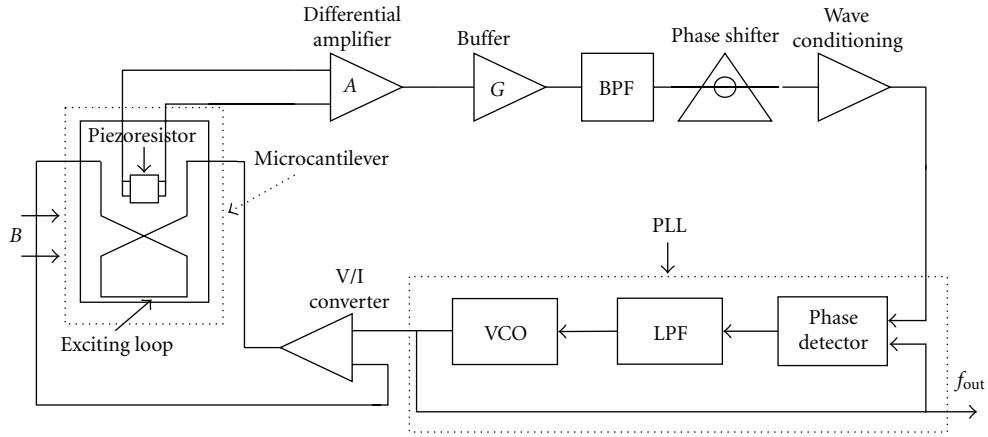

(a)

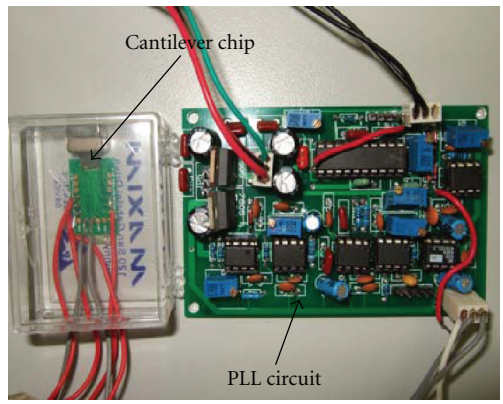

(b)

Figure 4: (a) Schematic phase-locked loop interface circuit for the micromechanical resonant sensor; (b) photograph of the interface circuit together with the cantilever sensor under testing.

resonance modes. Four types of integrated microcantilevers in four resonant modes are fabricated by micromachining techniques, which are the 1st bending-mode (shown in Figure 3(a)), the 2nd bending-mode (see Figure 3(b)), the 1st torsion-mode (Figure 3(c)), and the 2nd torsion-mode (Figure 3(d)). These four resonance modes are with the most possibility to be formed and practically used in dynamic microcantilever sensors. For practical experiments, the cantilevers for the 1st and 2nd torsional modes are optimally designed in a "*T*" shape structure and a Latin cross-shaped structure, respectively. These modifications in structure are due to some practical interests, such as a higher mass-sensing sensitivity, and an easier resonance excitation. By comparing the results obtained from the methods mentioned above, we expect to provide a guideline to help the designers to choose an optimized resonance mode for achieving high performance of microcantilever resonant sensors.

After theoretical analyses (with the details in [29]), we used professional microelectromechanical systems (MEMS) software, Coventor-ware, to simulate the four resonance modes. From the simulated results shown in Table 1, it can be concluded that, the damping characteristic of the torsional cantilever resonator is generally better than that of the flexural one, and the *Q*-factor of the cantilever resonator in a higher-order frequency mode is usually superior to that in a lower frequency mode. Therefore, it is suggested that optimal choice of the resonant mode is an effective method to improve the *Q*-factor of the resonant cantilever sensors. Among the integrated resonant microcantilever sensors fabricated and operated in our experiment, the 2nd torsion-mode one exhibits the best performance in terms of the highest *Q*-factor, the highest mass sensitivity, and the best sensing resolution.

To experimentally verify the analytical results for the resonant cantilever sensors with the 1st, 2nd flexural modes and the 1st, 2nd torsional modes, the four types of integrated microcantilevers are fabricated by using the micromaching techniques described above. The Lorentz-force resonance exciting and piezoresistive self-sensing elements are both on-chip integrated. With a network analyzer and a phase locked loop (PLL) interface circuit [30] shown in Figure 4, both open-looped and close-looped *Q*-factors are measured. With the results plotted and compared in Figure 5, the test for the four resonance modes show that a higher *Q* is obtained for a higher mode.

Table 1: Simulated results for a rectangular cantilevers resonating in different modes.

Mode	1st flexure	2nd flexure	1st torsion	2nd torsion
Resonant frequency (kHz)	52.3	328	293	924
Generalized mass (kg)	5.24e-11	5.23e-11	3.09e-11	2.58e-11
Damping coefficient C_d (μN/μm/s)	2.39e-8	2.37e-8	2.04e-8	1.80e-8
Damping ratio $\xi = C_d/2m\omega_0$	6.94e-4	1.09e-4	1.80e-4	6.01e-5
Quality factor $Q = 1/2\xi$	720	3587	2778	8319

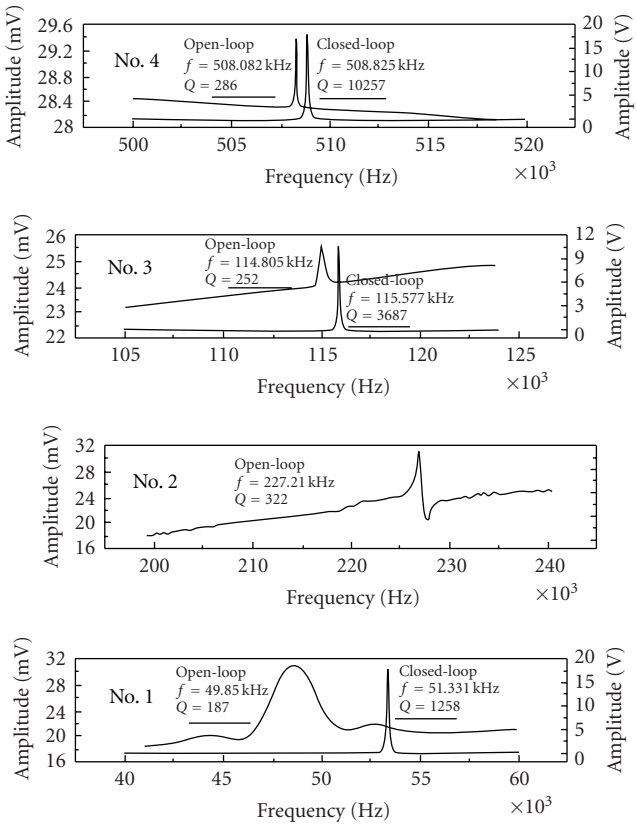

Figure 5: Measured amplitude-frequency responses for the 1st and 2nd flexural mode (no. 1 and 2), as well as, the 1st and 2nd torsion modes (no. 3 and 4) of cantilever sensors in the open-loop circuit (on the left side) and the closed-loop circuit (on the right side).

For further comparing the performance among the four types of microcantilever sensors, we implement a biotin-to-avidin specific binding experiment and frequency-shift test. Figure 6 shows the schematic process route for the immobilization of the biotin molecules and specific reaction with the avidin molecules. At first, biotin is anchored onto the Au sensing pads at the cantilever surface. The biotin is immobilized via a thiol-terminaled self-assembled molecular layer (SAM). Then, the cantilever is immersed into 0.05 mM solution of Au-particle labeled streptavidin for 20 minutes to complete the biotin-avidin specific hybridization. The tested resonant frequency shift of the cantilevers versus specific biologic hybridization is shown in Figure 7. When

Table 2: Measured mass induced frequency shift, mass sensitivity, Allan variance (a standard parameter to evaluate resonant-frequency instability over a certain period of time) and sensing resolution for different modes of the cantilevers. The designed mass sensitivity, the calculated Allan variables based on measured frequency stability, and the finally obtained mass-sensing resolution based on the Allan variables analysis, are all listed for the corresponding cantilevers in corresponding resonant modes.

Cantilever type	No. 1	No. 2	No. 3	No. 4
Δf (Hz)	57.5	591.2	443	2330
Sensitivity (Hz/pg)	0.33	4.3	0.9	5.1
Allan variance	2.1e-6	3.3e-7	7.6e-7	1.8e-7
Mass resolution (fg)	313	29	23	9

the absorbed mass, Δm, is smaller enough compared with the mass of the cantilever, the mass sensing sensitivity can be expressed as

$$S = \frac{\Delta f}{\Delta m} = \frac{1}{2}\frac{f_0}{m_{\text{eff}}}, \quad (1)$$

where Δf is the frequency shift, f_0 is the initiated resonance frequency, and m_{eff} is the effective mass of the cantilever. By using the equation, we can calculate the mass sensitivity of the integrated microcantilever sensors. As shown in Table 2, among the four cantilever sensors, the 2nd torsion-mode cantilever-sensor behaves as the highest frequency change of 2330 Hz. Moreover, a better mass-sensing resolution is obtained for a higher mode cantilever and the 2nd torsion-mode exhibits the best resolution of about 9 fg, that is, almost the mass of a single vaccinia virus. In Table 2, Allan variance values for all the modes are also provided, which is a standard parameter to evaluate resonant-requency instability over a certain period of time.

4. Trace-Level AFP Detection for Early-Stage Diagnosis of Heptocellular Carcinoma

The torsion-mode resonant cantilever, which features higher Q-factor value compared to conventional bending resonant mode, is used for trace level biochemical detection. For improving the detection limit, the resonant silicon resonant cantilever with the torsional mode is optimally designed and fabricated. Our experiments have shown that the sensor behaves an ultrasensitive detection capability for alpha-fetoprotein (AFP) antigen [31], which is one of the most

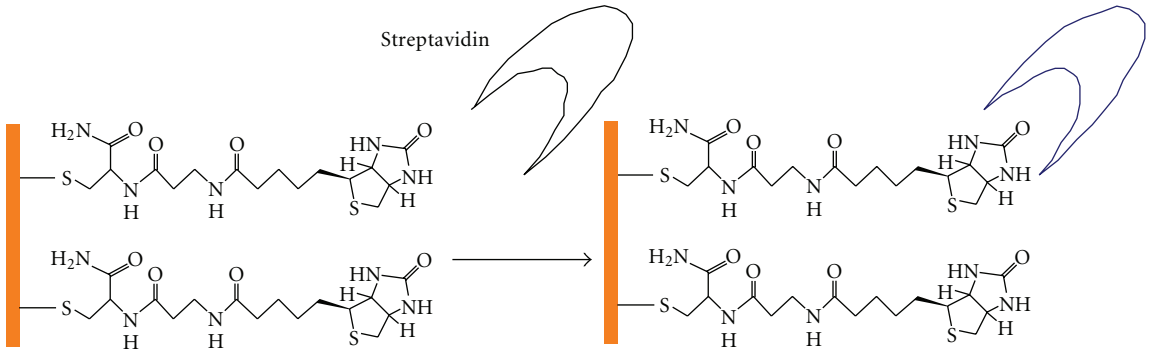

Figure 6: Schematic mechanism of the thiol-terminal biotin modified on the Au surface of the cantilever and the specific capture to gold-particle labeled streptavidin.

important tumor markers to indicate hepatocellular carcinoma (HCC) tumor spread and burden, cell differentiation, and aggressive potential [32]. It should be noticed that HCC is the fifth most common cancer worldwide and the third most common cause of cancer-related death, with about 500 000 new cases diagnosed in one year. For the purpose of early stage prognosis, an immunological sensor applied in detection of AFP would better feature the concentration detection limit of less than 10 ng/mL, that is, at ng/mL level [33]. Detailed technical treatments on the cantilever and the sensing experiments will be given in following subsections.

4.1. Immobilization of Self-Assembled Monolayer (SAM) Mediated mIg. To refresh the surface of the two Au sensing pads on the torsion-mode cantilever (see Figure 3(c)), the cantilever is pretreated in Piranha solution and then cleaned with deionized water. Together with the Au sensing pads, the cantilever is immersed in the SAM solution of 11-mercaptoundecanoic acid (MUA) at room temperature. Then the cantilever is sequentially rinsed by ethanol and deionized water. After dried by N_2 gas, the gold sensing surface has been modified by self-assembly of MUA. Before mIg immobilization, the cantilever is activated by DBPH [3,3-dithio-bis (propionic acid N-hydroxysuccinimide ester)] solution at room temperature. The cantilever is rinsed in ethanol and deionized water, then, dried by N_2 gas. Following these pretreatment steps, the cantilever is immersed into mIg solution for 1 hour. Then the cantilever is washed by the phosphate buffer solution of Phosphate Buffer Solution + Tween-20 (PBST) and deionized water. After linked to the Au surface, the mIg is suggested to be immediately used within a short period of time. When the mIg immobilized cantilever is restored under a low temperature of -20°C, it can still be used for immunodetection within several days.

4.2. Cantilever Surface Silanization and Avidin Recognition by Specific Reaction with Biotin. A mass adsorption can decrease the resonant frequency of a micaocantilever. It means that not only the specific analytes but also other containments nonspecifically attached to the cantilever surface can cause the frequency drop. Therefore, the specificity of the reaction should be enhanced and nonspecific molecular adsorption should be effectively depressed. More importantly, in addition to the influence to mass weighing, the surface nonspecific adsorption can increase the spring constant by stiffening the microcantilever, thereby, inducing an increase in the resonant frequency [34]. We have found that the cantilever-stiffening cross-effect can severely counteract and weaken the specific mass induced frequency-shift signal. The measurement results of the biotin-avidin specific reaction in Figure 8(a) show that the stiffening cross-signal even surpasses the mass signal and the frequency reversely increases. To avoid the cross-effect induced by nonspecific adsorption, we modify the cantilever surface to resist nonspecific protein or other molecule adsorption. Herein polyethylene glycol (PEG) is used as an effective reagent to eliminate unspecific adsorption. Considering that the surface of the microcantilever is silicon (at backside) and silicon dioxide (at front side), PEG is grafted on the cantilever surface with the format of PEG-silane. The detailed processes are given in next paragraph.

After pretreated with H_2O_2/H_2SO_4 solution and sequentially cleaned by ethanol and deionized water, the cantilever is immersed into a biotin-SH solution for 12 hours. After rinsed in ethanol and deionized water, the SiO_2 front side and silicon back side of the cantilever (except for the gold surface at the end pad for specific sensing) are both silanized by PEG-silane solution and cleaned by deionized water. This PEG-silane surface modification is used to effectively depress nonspecific adsorption of protein on the cantilever that can cause cross-talk to the specific reaction signal. The PEG-silane surface modification processes are sketched in Figure 9. After the cantilever is coated with BSA solution and rinsed by PBST/deionized water, the resonant frequency of the sensor is measured by a network analyzer. Then the biotin monolayer on the gold surface reacts with an avidin-Au solution for 30 minutes.

After the cantilever is rinsed by PBST/deionized water and dried by nitrogen gas, the resonant frequency shift is tested. Plotted in Figure 8(b), the testing results show that, with the PEG precoating technique used, the cantilever significantly decrease its resonant frequency according to the adsorbed mass of avidin-Au. This indicates that PEG-silane

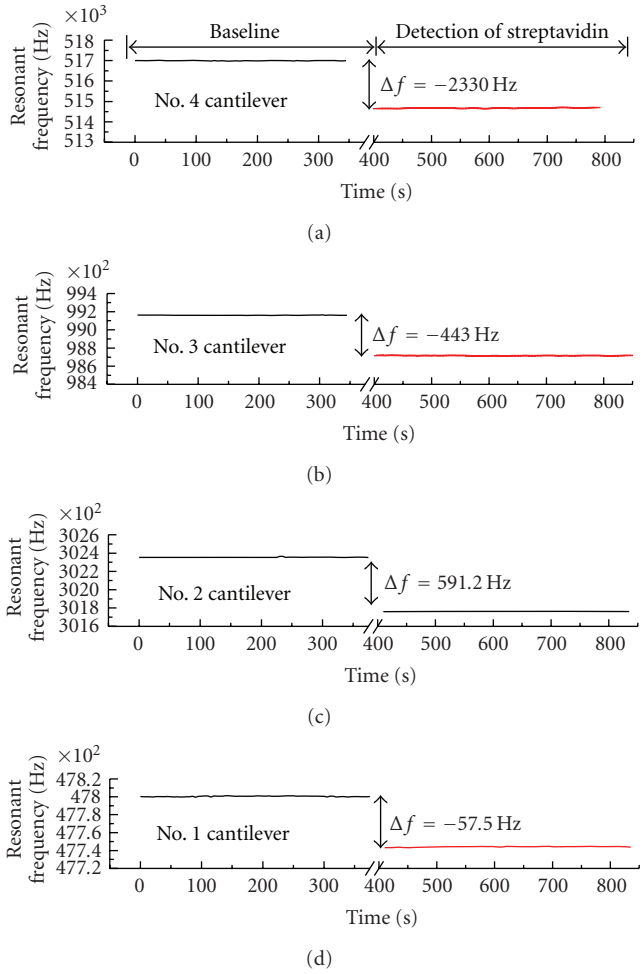

Figure 7: From bottom to top, the biotin-avidin specific hybridization induced frequency shifts are tested for the no. 1 cantilever in the 1st flexural mode, the no. 2 cantilever in the 2nd flexural mode, the no. 3 cantilever in the 1st torsional mode, and the no. 4 cantilever in the 2nd torsional mode, respectively.

can effectively resist nonspecific adsorption and improve the reliability of the sensor.

4.3. mIg Line Array Printing for Confirmation of AFP Specific Adsorption. To confirm that the antibody-antigen reaction has completed at the Au surface, monoclonal immunoglobulin (mIg) lines are arrayed on the patterned Au stripes of silicon chips. Since that there are discrete epitopes on the macromolecule outer surface, one macromolecular antigen can react with no less than two antibodies. Therefore, after the mIg captures one epitope of AFP, the other epitopes can be recognized by polyclonal immunoglobulins (pIg). Then the specifically adsorbed pIg is further reacted with the pIg Alkaline phosphatase-immunoglobulin (AP-Ig).

In this experiment, gold thin film stripes are electron-beam evaporated and patterned on a silicon chip whose surface was previously covered with SiO_2 by thermal oxidation. To validate the antibody-antigen specific reaction, the patterned Au stripes are firstly immobilized with mIg

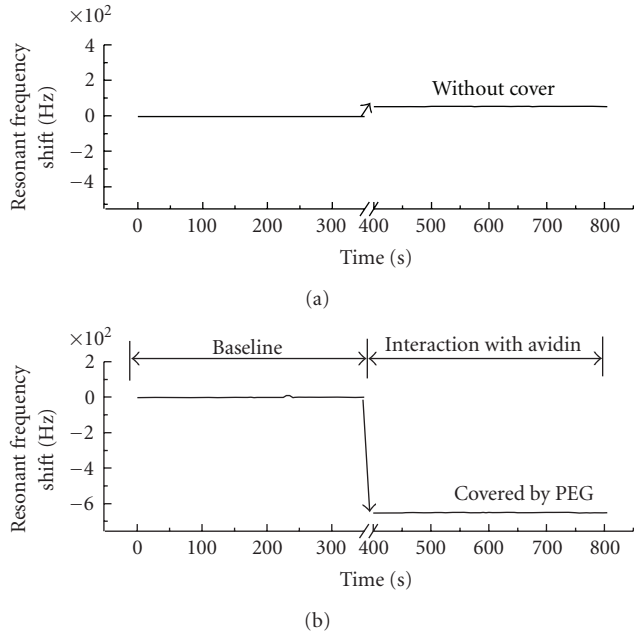

Figure 8: Comparison of the tested biotin-to-avidin reaction induced frequency shifts between the cantilever (a) without the PEG modification and (b) with the PEG-silane modification. By the PEG-saline modification method, the suppression of nonspecific adsorption effect on the detection performance is clearly indicated.

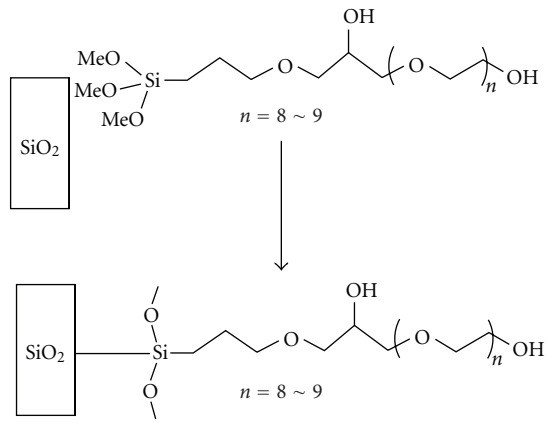

Figure 9: Cantilever-surface PEG-silane modification scheme for resisting against nonspecific protein adsorption.

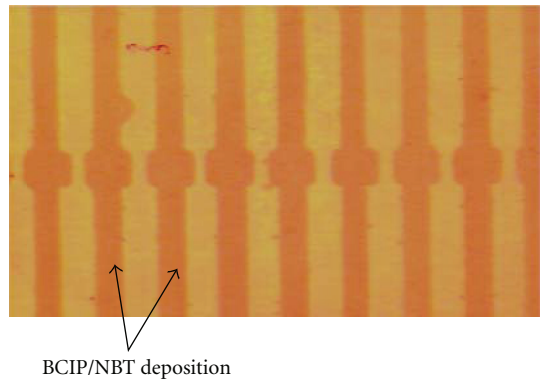

Figure 10: Microscope image of the BCIP/NBT deposition pattern.

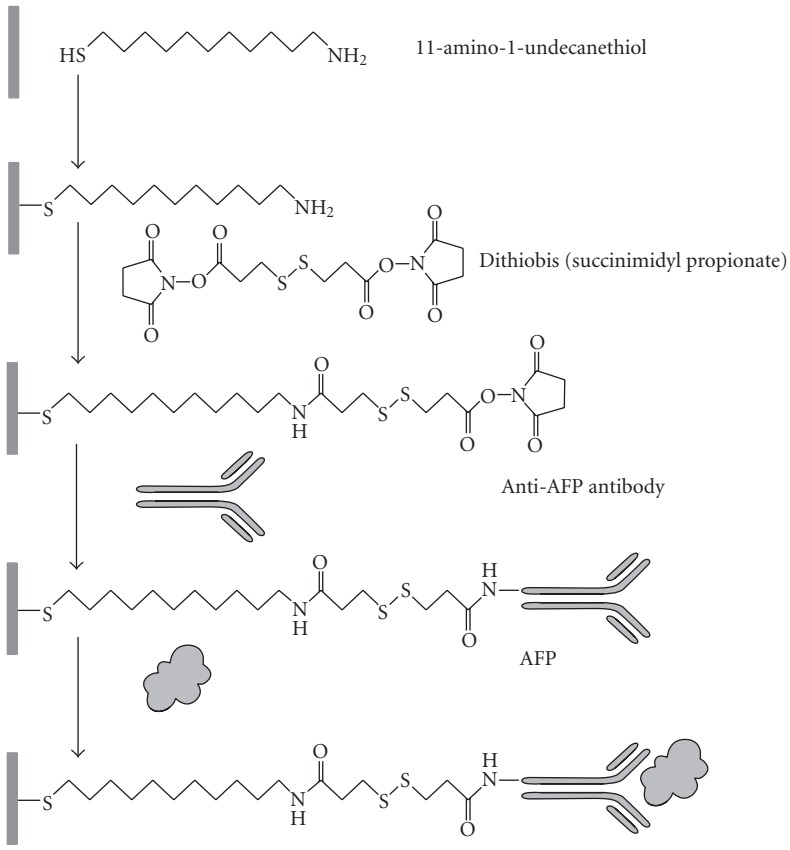

Figure 11: Serial immobilization processes of the anti-AFP antibody and the specific detection of AFP on the cantilever surface.

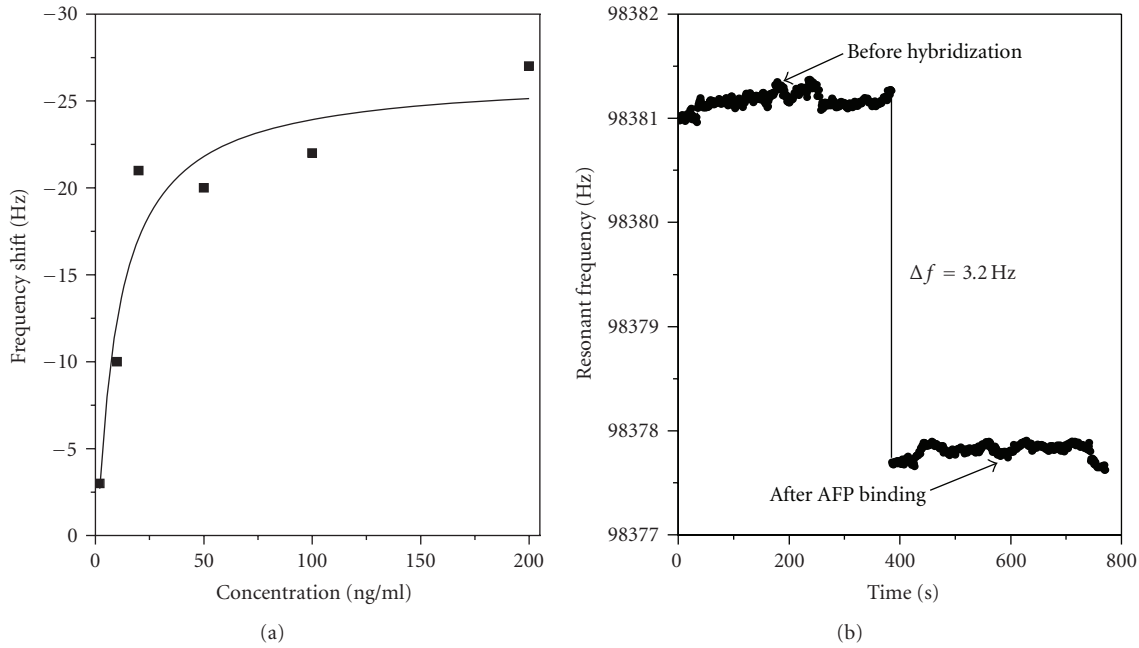

Figure 12: AFP testing results with the microcantilever sensor. (a) Sensor response signals in terms of various AFP concentrations. (b) Tested frequency shift for detection of ultralow AFP concentration of 2 ng/mL.

by using the processes described in previous subsection. Then the chip is immersed in bovine serum albumin (BSA) solution and, then, rinsed by PBST. After the Au stripes are coated by BSA, the chip is immersed in the AFP solution for 0.5–1 hour to complete the specific antigen-antibody reaction. Then, the chip is put in a pIg solution for 0.5 hour and washed again by PBST/deionized water. Then it is immersed in a pIg AP-Ig solution for 0.5 hour and washed by PBST/deionized water. Finally, the cantilever is put into the mixing solution of 5-bromo-4-chloro-3-indolyl-phosphate (BCIP) and Nitro-Blue-Tetrazolium (NBT) for 1 hour, and then, cleaned in deionized water and dried by nitrogen gas.

The Alkaline Phosphatase (AP) catalyses the complex of BCIP and NBT, resulting in that a colored deposition is formed on the surface for experimental observation under a microscope. The digital micrograph in Figure 10 shows that the deposition is only formed on the mIg lines, which indicates that the mIg does specifically capture AFP and the antibody-antigen reaction has occurred on the Au surface.

4.4. Recognition of AFP. The cantilever surface is cleaned and pretreated with H_2O_2/H_2SO_4 solution, then rinsed in ethanol/deionized water. After the SAM of MUA is formed on the Au end-pads of the cantilever, the cantilever surface is silanized by PEG-silane. The mIg is immobilized on top of the SAM of MUA. The steps of the mIg immobilization have been described above, thus, are not repeated again. Before measurement of the initial resonant-frequency, the cantilever is coated with BSA solution. Then the cantilever is used to recognize AFP. After the cantilever reacts with AFP of a certain concentration, it is washed by PBST and deionized water. After drying by nitrogen, the frequency shift of the cantilever is measured in lab air. The sequential processes of immobilization of mIg and the specific reaction with AFP are schematically demonstrated in Figure 11.

Prior to the reaction with AFP, the initial frequency of the microcantilevers is measured as the referential frequency. After the specific binding, AFP antigen is absorbed to the Au pads that have been previously immobilized with the anti-AFP antibody. Therefore, the mass addition of the microcantilever decreases the resonant frequency. Figure 12(a) shows the experimentally obtained frequency shifts in terms of various concentrations of AFP solution (i.e., 0 ng/mL, 2 ng/mL, 10 ng/mL, 20 ng/mL, 50 ng/mL, 100 ng/mL, and 200 ng/mL). The detectable concentration of AFP is better that the cut-off value of 15–20 ng/mL, which is widely accepted as one of the indicators of HCC. In the case of no AFP, there is no significant frequency shift. Since that the range of AFP levels for hepatitis patients with or without HCC normally overlaps, the normal referential range of AFP should be lower than 10 ng/mL. The frequency shift in Figure 12(b) indicates that the signal noise limited AFP detecting resolution can be better than 2 ng/mL Phosphate Buffer Solution (PBS) solution, the detection limit of the developed cantilever sensor can be considered at ng/mL level. Therefore, the microcantilevers have the ability to detect HCC at early stage, therefore has the potential to be applied in clinical assay.

5. Conclusions

Resonant microcantilecver sensors have been intensively developed in Chinese Academy of Sciences in recent years. The optimization of resonance modes is studied for enhancing the detecting resolution to trace level targeted molecules. Both resonance exciting and signal pick-up elements are integrated in the cantilevers for low-cost portable applications. Multiple and localized self-assembly techniques are developed to enhance sensing specificity and depress cross-talk noise. Ultralow concentration biological detection has been successful realized that shows great promise in future biomedical applications.

Acknowledgments

This research is supported by the NSFC Project under contract no. 60725414, the Chinese 973 Program (2006CB300405), and Chinese 863 Project (2006AA04Z365). Xinxin Li also appreciates the financial support of the NSFC Project (60721004).

References

[1] N. V. Lavrik, M. J. Sepaniak, and P. G. Datskos, "Cantilever transducers as a platform for chemical and biology sensors," *Review of Scientific Instruments*, vol. 75, pp. 2229–2253, 2004.

[2] J. R. Barnes, R. J. Stephenson, M. E. Welland, C. Gerber, and J. K. Gimzewski, "Photothermal spectroscopy with femtojoule sensitivity using a micromechanical device," *Nature*, vol. 372, no. 6501, pp. 79–81, 1994.

[3] D. R. Baselt, G. U. Lee, K. M. Hansen, L. A. Chrisey, and R. J. Colton, "A high-sensitivity micromachined biosensor," *Proceedings of the IEEE*, vol. 85, no. 4, pp. 672–680, 1997.

[4] J. Fritz, M. K. Baller, H. P. Lang, et al., "Translating biomolecular recognition into nanomechanics," *Science*, vol. 288, no. 5464, pp. 316–318, 2000.

[5] T. Thundat, E. Finot, Z. Hu, R. H. Ritchie, G. Wu, and A. Majumdar, "Chemical sensing in Fourier space," *Applied Physics Letters*, vol. 77, no. 24, pp. 4061–4063, 2000.

[6] A. Boisen, J. Thaysen, H. Jensenius, and O. Hansen, "Environmental sensors based on micromachined cantilevers with integrated read-out," *Ultramicroscopy*, vol. 82, no. 1–4, pp. 11–16, 2000.

[7] T. Thundat, E. A. Wachter, S. L. Sharp, and R. J. Warmack, "Detection of mercury vapor using resonating microcantilevers," *Applied Physics Letters*, vol. 66, pp. 1695–1697, 1995.

[8] B. Ilic, D. Czaplewski, M. Zalalutdinov, et al., "Single cell detection with micromechanical oscillators," *Journal of Vacuum Science and Technology B*, vol. 19, no. 6, pp. 2825–2828, 2001.

[9] A. Gupta, D. Akin, and R. Bashir, "Single virus particle mass detection using microresonators with nanoscale thickness," *Applied Physics Letters*, vol. 84, no. 11, pp. 1976–1978, 2004.

[10] T. Ono, X. Li, H. Miyashita, and M. Esashi, "Mass sensing of adsorbed molecules in sub-picogram sample with ultrathin silicon resonator," *Review of Scientific Instruments*, vol. 74, no. 3, pp. 1240–1243, 2003.

[11] K. L. Ekinci, X. M. H. Huang, and M. L. Roukes, "Ultrasensitive nanoelectromechanical mass detection," *Applied Physics Letters*, vol. 84, no. 22, pp. 4469–4471, 2004.

[12] Z. Djurič, "Mechanisms of noise sources in microelectromechanical systems," *Microelectronics Reliability*, vol. 40, no. 6, pp. 919–932, 1999.

[13] C. Hagleitner, A. Hierlemann, D. Lange, et al., "Smart single-chip gas sensor microsystem," *Nature*, vol. 414, no. 6861, pp. 293–296, 2001.

[14] E. Forsen, G. Abadal, S. Ghatnekar-Nilsson, et al., "Ultrasensitive mass sensor fully integrated with complementary metal-oxide-semiconductor circuitry," *Applied Physics Letters*, vol. 87, no. 4, Article ID 043507, 3 pages, 2005.

[15] R. Berger, E. Delamarche, H. P. Lang, et al., "Surface stress in the self-assembly of alkanethiols on gold," *Science*, vol. 276, no. 5321, pp. 2021–2024, 1997.

[16] T. Thundat, R. J. Warmack, G. Y. Chen, and D. P. Allison, "Thermal and ambient-induced deflections of scanning force microscope cantilevers," *Applied Physics Letters*, vol. 64, no. 21, pp. 2894–2896, 1994.

[17] M. Tortonese, R. C. Barrett, and C. F. Quate, "Atomic resolution with an atomic force microscope using piezoresistive detection," *Applied Physics Letters*, vol. 62, no. 8, pp. 834–836, 1993.

[18] J. Thaysen, A. Boisen, O. Hansen, and S. Bouwstra, "Atomic force microscopy probe with piezoresistive read-out and a highly symmetrical Wheatstone bridge arrangement," *Sensors and Actuators A*, vol. 83, no. 1, pp. 47–53, 2000.

[19] P. A. Rasmussen, J. Thaysen, S. Bouwstra, and A. Boisen, "Modular design of AFM probe with sputtered silicon tip," *Sensors and Actuators A*, vol. 92, no. 1–3, pp. 96–101, 2001.

[20] A. Kooser, R. L. Gunter, W. D. Delinger, T. L. Porter, and M. P. Eastman, "Gas sensing using embedded piezoresistive microcantilever sensors," *Sensors and Actuators B*, vol. 99, no. 2-3, pp. 474–479, 2004.

[21] H. Jensenius, J. Thaysen, A. A. Rasmussen, L. H. Veje, O. Hansen, and A. Boisen, "A microcantilever-based alcohol vapor sensor-application and response model," *Applied Physics Letters*, vol. 76, no. 18, pp. 2615–2617, 2000.

[22] L. A. Pinnaduwage, D. L. Hedden, A. Gehl, et al., "A sensitive, handheld vapor sensor based on microcantilevers," *Review of Scientific Instruments*, vol. 75, no. 11, pp. 4554–4557, 2004.

[23] M. H. Bao, "Micro mechanical transducer," in *Handbook of Sensors and Actuators*, S. Middelhoek, Ed., Elsevier, Amsterdam, The Netherlands, 2000.

[24] D. Jin, X. Li, H. Bao, et al., "Integrated cantilever sensors with a torsional resonance mode for ultraresoluble on-the-spot bio/chemical detection," *Applied Physics Letters*, vol. 90, no. 4, Article ID 041901, 2007.

[25] D. Jin, X. Li, J. Liu, et al., "High-mode resonant piezoresistive cantilever sensors for tens-femtogram resoluble mass sensing in air," *Journal of Micromechanics and Microengineering*, vol. 16, no. 5, pp. 1017–1023, 2006.

[26] T. R. Albrecht, P. Grütter, D. Horne, and D. Rugar, "Frequency modulation detection using high-Q cantilevers for enhanced force microscope sensitivity," *Journal of Applied Physics*, vol. 69, no. 2, pp. 668–673, 1991.

[27] P. S. Waggoner and H. G. Craighead, "Micro- and nanomechanical sensors for environmental, chemical, and biological detection," *Lab on a Chip*, vol. 7, no. 10, pp. 1238–1255, 2007.

[28] T. Kunstmann, A. Schlarb, M. Fendrich, D. Paulkowski, Th. Wagner, and R. Möller, "Combined normal and torsional mode in frequency-modulation atomic force microscopy for lateral dissipation measurement," *Applied Physics Letters*, vol. 88, no. 15, Article ID 153112, 2006.

[29] X. Xia and X. Li, "Resonance-mode effect on microcantilever mass-sensing performance in air," *Review of Scientific Instruments*, vol. 79, no. 7, Article ID 074301, 2008.

[30] X. Xia, Z. Zhang, and X. Li, "A Latin-cross-shaped integrated resonant cantilever with second torsion-mode resonance for ultra-resoluble bio-mass sensing," *Journal of Micromechanics and Microengineering*, vol. 18, no. 3, Article ID 035028, 2008.

[31] Z. Zhang, H. Bao, H. Yu, and X. Li, "Ng/ml-level alpha-fetoprotein immunodetection with torsion-mode cantilever sensors for early-stage heptocellular carcinoma diagnosis," in *Proceedings of the 14th International Conference on Solid-State Sensors, Actuators and Microsystems (TRANSDUCERS '07)*, pp. 1785–1788, Lyon, France, June 2007.

[32] L. Zhou, J. Liu, and F. Luo, "Serum tumor markers for detection of hepatocellular carcinoma," *World Journal of Gastroenterology*, vol. 12, no. 8, pp. 1175–1181, 2006.

[33] B. J. McMahon, L. Bulkow, A. Harpster, et al., "Screening for hepatocellular carcinoma in Alaska natives infected with chronic hepatitis B: a 16-year population-based study," *Hepatology*, vol. 32, no. 4, pp. 842–846, 2000.

[34] G. Y. Chen, T. Thundat, E. A. Wachter, and R. J. Warmack, "Adsorption-induced surface stress and its effects on resonance frequency of microcantilevers," *Journal of Applied Physics*, vol. 77, no. 8, pp. 3618–3622, 1995.